Flow Field of Truncated Spherical Turrets

Kevin M. Albarado[1] and Amelia Williams[2]
Aerospace Engineering, Auburn University, Auburn, AL, 36849

Truncated spherical turrets are used to house cameras and sensors in most airborne surveillance platforms. Because of the geometrical changes, flow in the vicinity of the attachment point is significantly distorted and fraught with steeper density gradients that can result in optical degradation of the images and beam propagation in applications such as tactical lasers. Tests were conducted in the water tunnel and the wind tunnel to determine the flow field features. Ongoing flow visualization using LIF techniques and PIV measurements in the water tunnel are presented and discussed. Also presented are the wind tunnel results of drag measurements.

Nomenclature

AoA	=	angle of attack
C_d	=	drag coefficient
CCD	=	charged coupled device
LIF	=	laser induced fluorescence
PIV	=	particle image velocimetry

I. Introduction

Truncated spherical turrets are used to house surveillance equipment such as cameras and sensors in airborne reconnaissance vehicles. Examples of aerial vehicles carrying tactical turrets are reconnaissance airplanes as well as various civilian, commercial, and military helicopters. The turrets are mounted forward of the aircraft or on the undercarriage. For aero-optical applications such as tactical airborne lasers, these turrets have a flat window. This unique geometry is what is referred to as a truncated sphere. Due to the sharp geometrical changes, flow in the vicinity of the attachment point is significantly disrupted and fraught with steeper density gradients resulting in optical degradation in imaging and beam propagation in tactical lasers. One particular flow characteristic of a blunt or flat nose body is the formation of streamwise vortices on the leading surface[2]. Upstream of the leading edge, when viewed in the plane of symmetry, the new bifurcation point forms near the attachment point. For spheres, the bifurcation point occurs on the leading edge of the body. However, for truncated spheres, the bifurcation occurs upstream of the body due to flow entrainment in this region. This entrained flow can cause image distortion in camera surveillance equipment, and beam propagation, wave-front jitter, and intensity loss in laser-optic surveillance sensors. The objective of the following study is to determine the flow field characteristics which are responsible for aero-optical distortions on the surveillance equipment. The flow about four spherical bodies at varying angles of attack from 0-15° was therefore investigated.

II. Experimental Apparatus and Methods

The test models were acrylic spheres painted black to decrease laser interference. The models tested were varied in truncation from 2.5% to 10%.

A. Experimental Setup in the Water Tunnel

Water tunnel tests were performed the Auburn University 18 in. x 18 in. water tunnel. The models were sting mounted as shown in Fig. 1. The Reynolds number for the flow visualization was limited to 18,700 based on the sphere diameter. Three flow visualization techniques were used to determine the flow characteristics. One technique introduced hydrogen bubbles upstream of the body using a platinum wire. A high powered laser was used to illuminate the hydrogen bubbles. This technique was used on each model at -15°, -7.5°, 0°, +7.5°, and +15°. Although the models are spherical, flow around the top surface was not visible due to the body blocking the laser

---

[1] Undergraduate Research Assistant, Aerospace Engineering, and AIAA Member.
[2] Undergraduate Research Assistant, Aerospace Engineering, and AIAA Member.

sheet. By running tests at both positive and negative angles of attack, a full profile of the flow characteristics was determined. Another flow visualization technique used was LIF. LIF was used to determine flow characteristics on the leading surface of the bodies as well as to determine wake characteristics. LIF and Hydrogen bubble flow visualization techniques are limited to qualitative analysis and are capable of only showing instantaneous flow characteristics.

For quantitative analysis to determine flow field characteristics, PIV measurements were made. PIV is a non-intrusive technique for data acquisition as well as flow visualization. PIV measures the flow of seeded particles in the fluid over time. The particles are illuminated periodically with a high intensity laser, and simultaneously a CCD camera captures an image. PIV works by taking a specified series of images, and tracking each individual particle to determine velocity characteristics. Preliminary results determined that the number of images to correlate needed to be around 25 images in order to properly model the overall flow characteristics. Seeding particles used for PIV were silver coated hollow glass spheres with an average diameter of 20 μm. Statistics were calculated from a 32 x 32 pixel interrogation window.

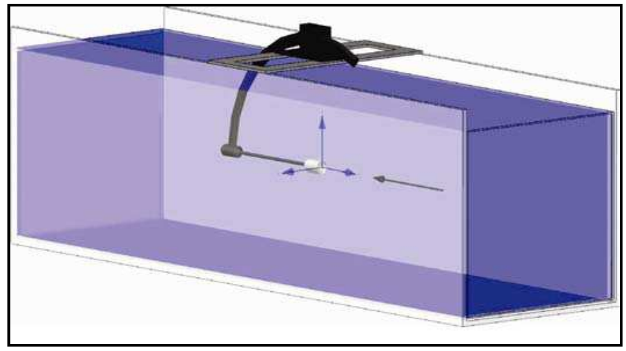

Figure 1: Water Tunnel Setup

B. Experimental Setup in the Wind Tunnel

Aerodynamic testing was performed in the Auburn University 3 ft. x 4 ft. Closed Circuit Subsonic Wind Tunnel. The models were sting mounted to a pyramidal balance. Drag forces were calculated at Re = 75000, 110000, 145000, and 180000. Results were compared to a sphere with no truncation. In order to more accurately model real world application flow characteristics, and due to physical limitations of the wind tunnel, drag was also calculated with a transition strip on the model. Tripping flow by use of a transition strip from laminar boundary layer to turbulent boundary layer "leads to later separation and drag reduction even at much lower Reynolds numbers."[1] Models were tested at 0°, 7.5°, and 15° AoA.

III. Results and Discussion

A. Flow Visualization Results

Hydrogen bubble and LIF provided images of instances in the cycles of flow over truncated spherical turrets. In these instances, counter-rotating vortices, ring vortices, and stagnant flow buildup could be viewed. Each model exhibited similar instantaneous characteristics at each respective AoA. For 0° AoA, Fig. 2 shows entrained flow on the 2.5% truncation model. Also on the 2.5% truncation model at a later instance, two counter-rotating vortices can be viewed, as shown in Fig. 3. On the 10% truncation model, an LIF image, shown in Fig. 4, also shows two counter-rotating vortices. Figure 5 is an LIF image on the same model showing the bifurcation point forward of the model. These topologies provide an insight to how the flow reacts instantaneously to a truncated sphere. At positive and negative AoA, a much different cycle occurs. In Figure 6, a ring vortex forms on the truncated surface, causing early flow separation on the lower surface. In Fig. 7, the ring vortex has broken down, and flow separates from the model much further downstream. The separation point oscillated forward and aft on the model in this manner for all models at AoA. Figure 8 further explains this behavior. A ring vortex first forms on the truncated surface, accelerating the flow, causing separation at the edge of the truncated surface. Over time the ring vortex builds until the entrained flow is ejected. This causes the separation point to move further down the model.

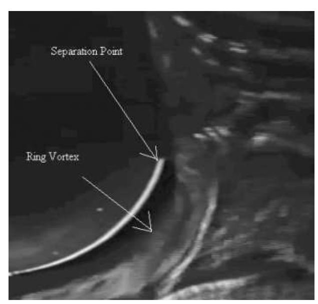

Figure 6. Ring Vortex, Early Separation

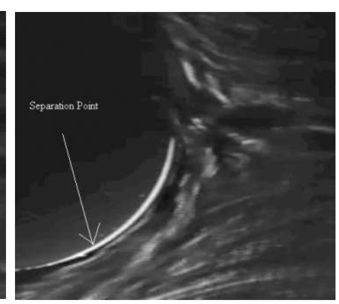

Figure 7. Ring Vortex, Late Separation

B. PIV Data Acquisition

Using PIV, a velocity profile developed, and a C_p distribution was plotted. The results for each model at each AoA can be found in Fig. 9 - 28. Red regions represent a value of C higher than freestream C, indicative of stagnant flow; green regions indicate values of C equal to freestream flow; blue regions represent regions of C values less than that of freestream flow, indicative of accelerated flow. Comparing Fig. 9, 14, 19, and 24, the region of stagnant flow on the surface increased with increasing truncation. When AoA is increased to 7.5° and 15°, the same trend occurs. This trend was expected since the total wetted area of the flat surface increases with increased truncation. As AoA increases, the wetted area of the flat surface decreases, and so the region of the stagnant flow decreases in size, as evidenced by Fig. 24 & 26.

C. Aerodynamic Data Acquisition

Drag measurements were made under laminar flow at Reynolds numbers of 75000, 110000, 145000, and 180000. The Reynolds number remained under the critical value and therefore a transition strip was applied. The tests were then performed at the same Reynolds numbers with the transition strip to induce turbulent flow. At 0° AoA, the overall trend was that drag increased with an increase in Reynolds number. The turbulent case had less drag overall than the laminar case. Referencing to the data in Table 1, C_d values for the laminar case range from .14 to .24. For the turbulent case, as shown in Table 2, C_d values range from .12 to .20. This corresponds to approximately a 25% reduction in drag by simply inducing turbulent flow. When comparing the truncated spheres to the smooth sphere in the laminar flow, the drag coefficient was significantly higher. However, as Reynolds number increased, the drag coefficients of the truncated spheres approached that of the smooth sphere.

IV. Conclusion

From the results collected, causes adverse pressure gradients on the leading surface of the body. Based on LIF and hydrogen bubble images gathered, many complex topologies were observed. These geometries include bifurcating flow with counter-rotating vortices, entrained flow, and ring vortices. When ring vortices form on the leading surface, flow separates almost immediately. As the ring vortex builds up, the separation point moves further downstream until the vortex bursts, at which point the separation point is at its maximum distance away from the leading edge. PIV results averaged the cycles of flow geometries, and compiled a single image to describe the flow. Based on PIV results, it was concluded that flow did indeed stagnate at the leading edge. The size of the stagnation region increased with the size of the truncation, which correlates to the wetted area of the flat surface at 0° AoA. Similarly, the stagnation region increased with truncation at an AoA, however, this region was noticeably smaller than the case when AoA was 0°. The aerodynamic tests validated the observed data. The drag coefficient increased with truncation, and decreased with AoA. In order to properly model the flow properties similar to real world applications, turbulent flow was induced and compared to laminar values. The drag coefficient for turbulent flow was significantly less than that of laminar flow.

Truncating a sphere causes a penalty in drag. Truncating the spheres also complexes the flow around the flat surface. It also causes instabilities in the flow. When averaged out, the overall effect of the truncation is a stagnant flow buildup on the leading surface. In an applicable case, say when used to house surveillance cameras and sensors, this flow buildup could cause image distortion, beam propagation, wave-front jitter, and intensity loss. Next phase in this research is to study the aero-optical interactions that occur when oncoming flow passes over these laser turrets.

Appendix A: Hydrogen Bubble and LIF

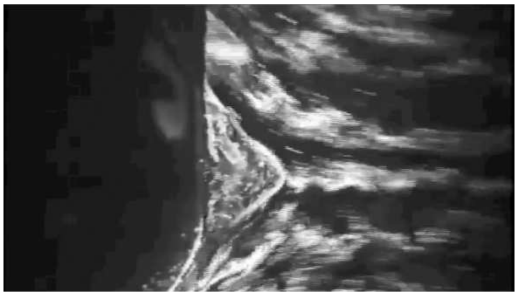

Figure 2. 2.5% Truncation, Entrainment

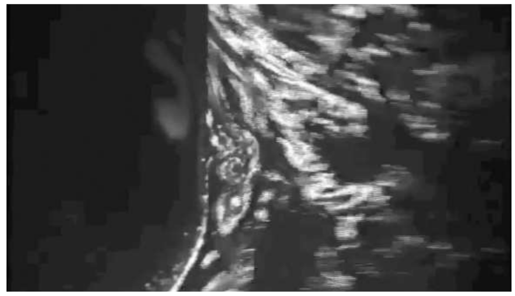

Figure 3. 2.5% Truncation, Counter-Rotation

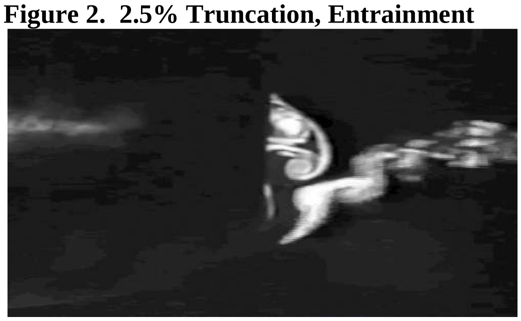

Figure 4. 10% Truncation, Counter-Rotation

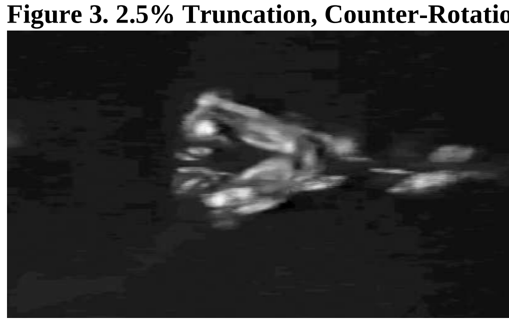

Figure 5. 10% Truncation, Bifurcation

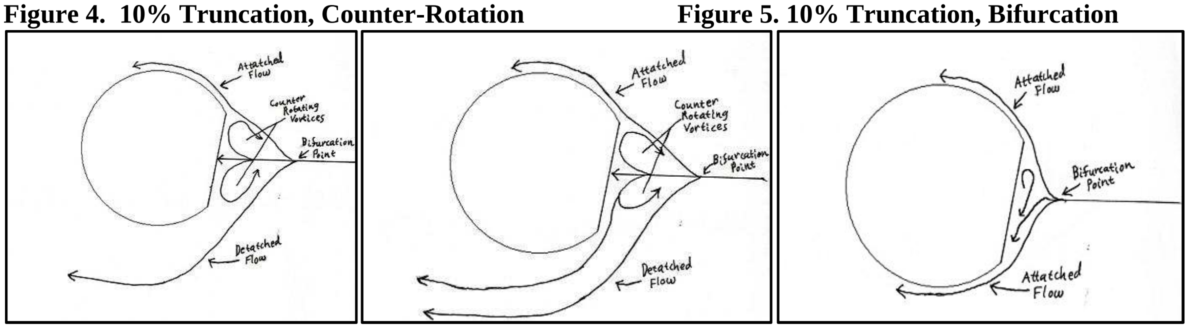

Figure 8. Ring Vortex Breakdown Diagram

Appendix B: PIV Results

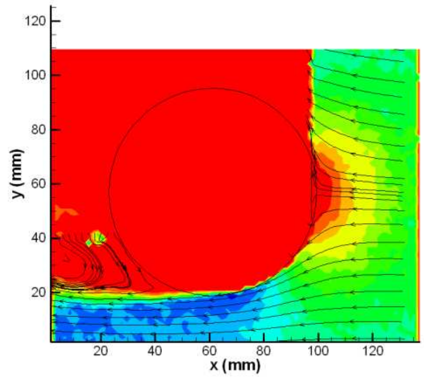

Figure 9. 2.5% Truncation, 0° AoA

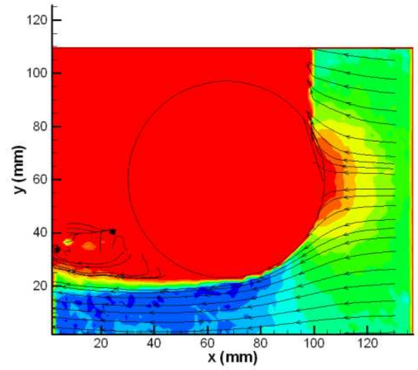

Figure 10. 2.5% Truncation, 7.5° AoA

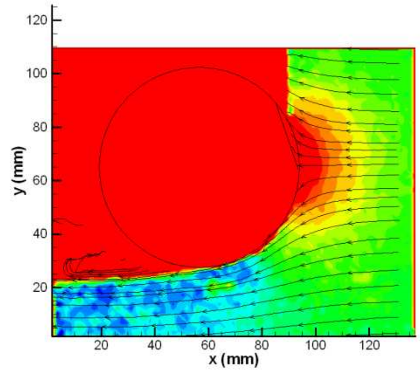

Figure 11. 2.5% Truncation, 15° AoA

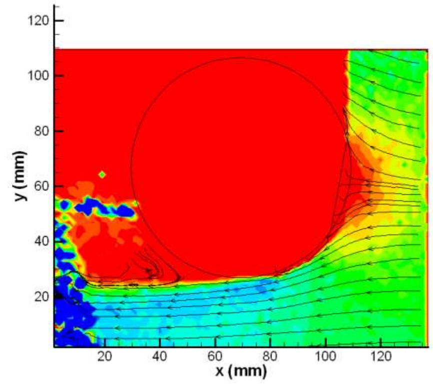

Figure 12. 2.5% Truncation, -7.5° AoA

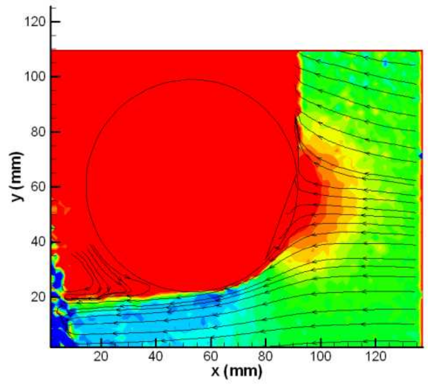

Figure 13. 2.5% Truncation, -15° AoA

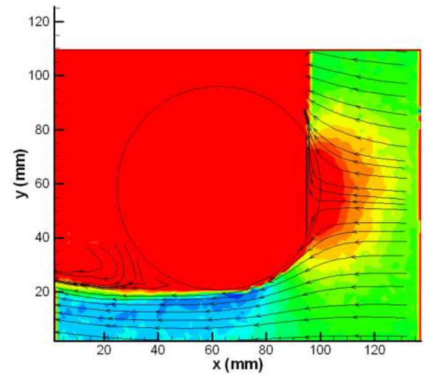

Figure 14. 5% Truncation, 0° AoA

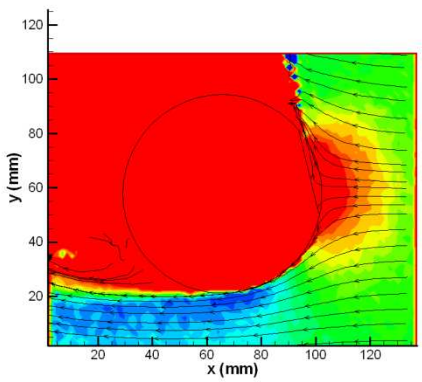

Figure 15. 5% Truncation, 7.5° AoA

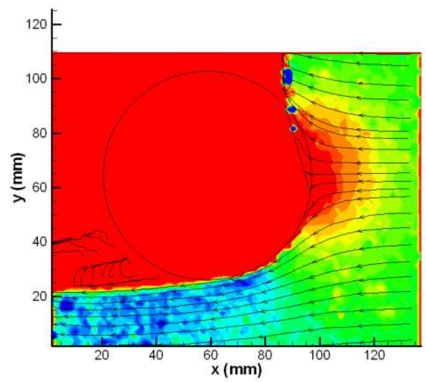

Figure 16. 5% Truncation, 15° AoA

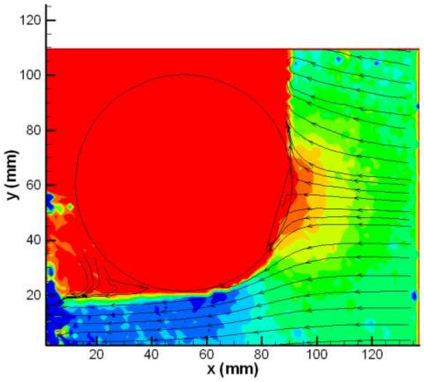

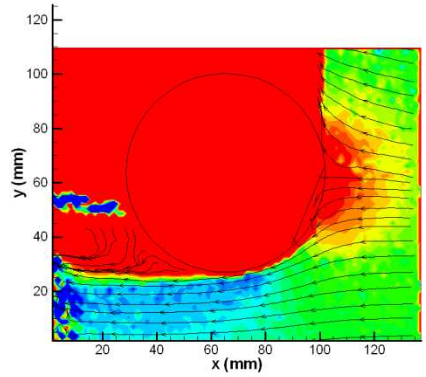

Figure 17. 5% Truncation, -7.5° AoA **Figure 18. 5% Truncation, -15° AoA**

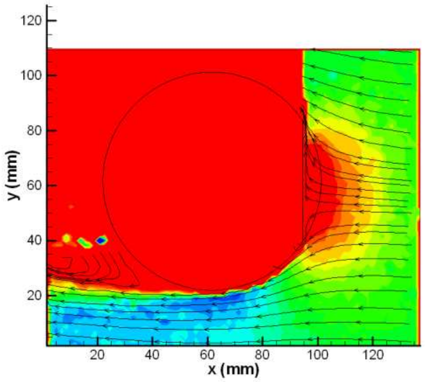

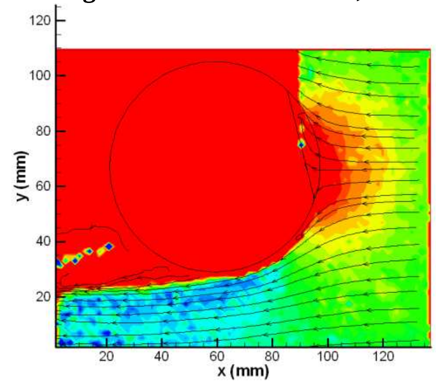

Figure 19. 7.5% Truncation, 0° AoA **Figure 20. 7.5% Truncation, 7.5° AoA**

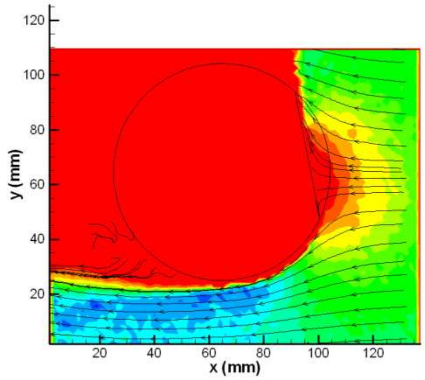

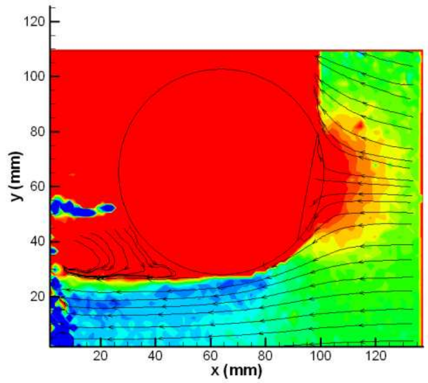

Figure 21. 7.5% Truncation, 15° AoA **Figure 22. 7.5% Truncation, -7.5° AoA**

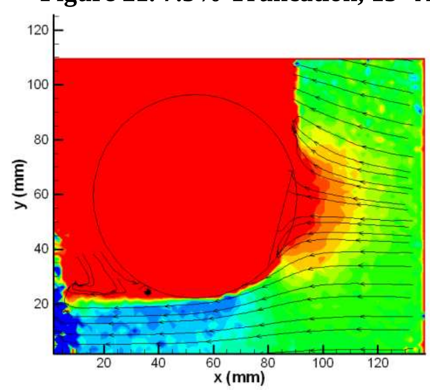

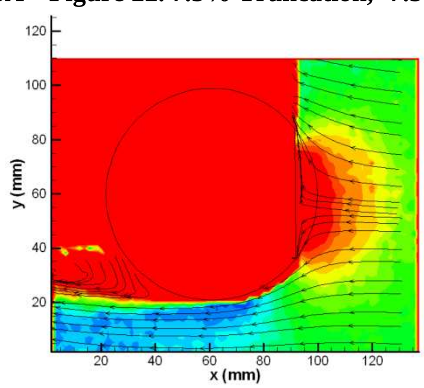

Figure 23. 7.5% Truncation, -15° AoA **Figure 24. 10% Truncation, 0° AoA**

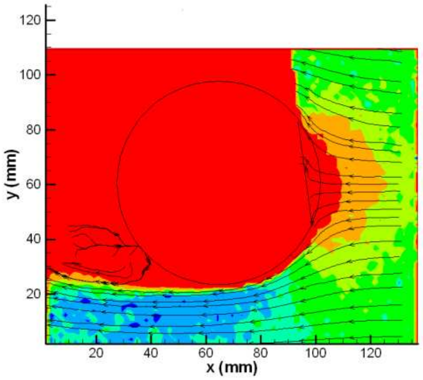

Figure 25. 10% Truncation, 7.5° AoA

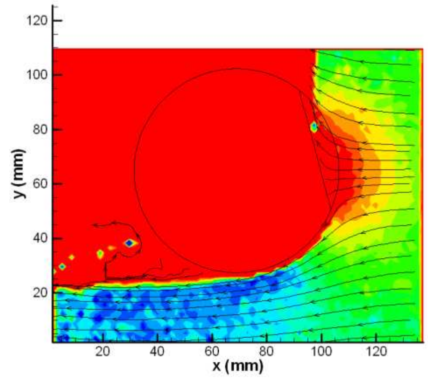

Figure 26. 10% Truncation, 15° AoA

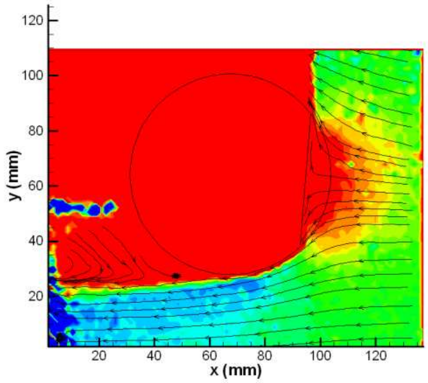

Figure 27. 10% Truncation, -7.5° AoA

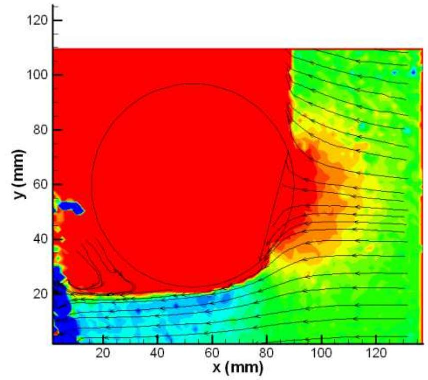

Figure 28. 10% Truncation, -15° AoA

Appendix C: Aerodynamic Results

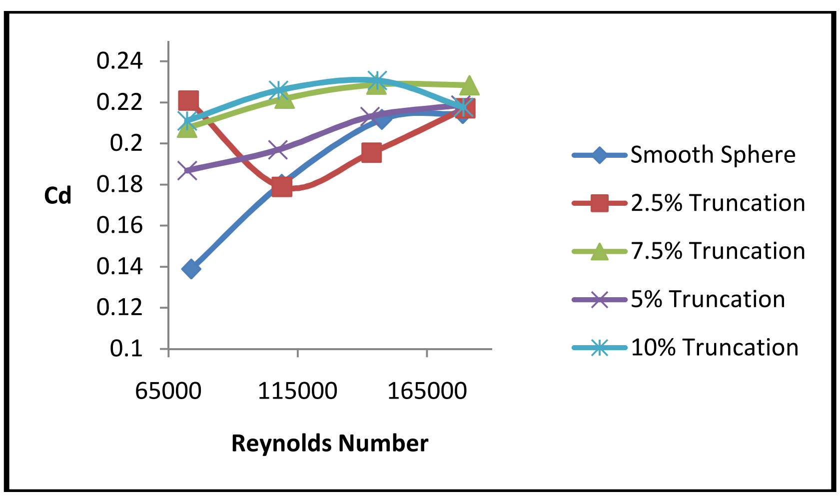

Table 1. Cd vs. Reynolds number in Laminar Flow

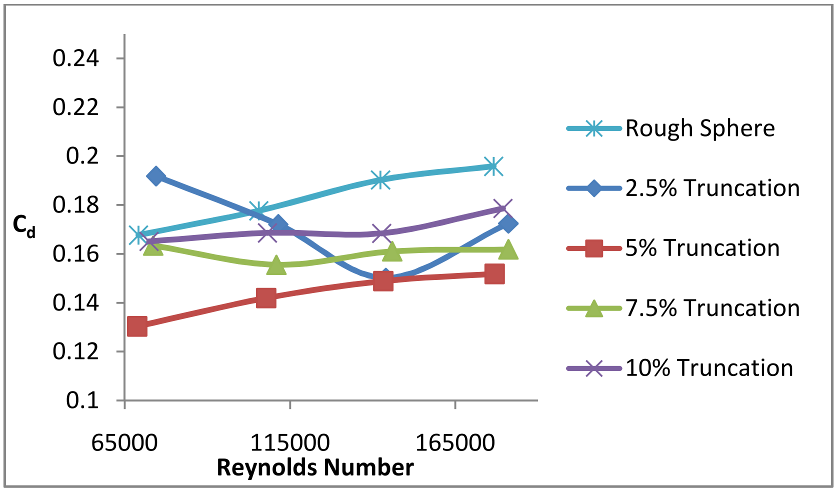

Table 2. Cd vs. Reynolds Number in Turbulent Flow

References

[1]Bakić, V., and M. Perić. "Visualization of Flow Around Sphere for Reynolds Numbers Between 22 000 and 400 000." Thermophysics and Aeromechanics, 2005, Vol. 12, No.3. 2005. 28 Aug. 2008 < http://vin.bg.ac.yu/~bakicv/bakic-paper1.pdf >.

[2]Pantelatos, D.K., and D.S. Mathioulakis. "Experimental flow study over a blunt-nosed axisymmetric body at incidence." Journal of Fluids and Structures 10 (2004) 1103-1115. 2008. Elsevier. Science Direct. Auburn University Library, Auburn, AL. 29 Aug. 2008.